Heart Rate Variability from Imaging

Integrated 1st Cycle Project in Biological Engineering

João Pires de Azevedo Teixeira dos Prazeres 103495
Bachelors Degree in Biological Engineering
Instituto Superior Técnico

Supervisors: Prof. João Miguel Raposo Sanches
Diogo Ramalho

***Abstract*—Depressive disorders are among the leading causes of disability worldwide. Remote psychiatric consultation, also known as telepsychiatry, can improve access to mental health services, reduce waiting times and ease the burden on healthcare systems. New digital-based tools that provide relevant depression biomarkers, such as speech analysis, eye-blinking rate and heart rate variability, could facilitate the diagnosis of depressive disorders. This work focuses on optimizing a state-of-the-art remote photoplethysmography model to provide heart rate variability features in a telepsychiatry setting. The model was validated using an available video dataset. For the time domain heart rate variability features SDNN (standard deviation of NN intervals) and RMSSD (root mean square of successive square differences), the mean errors obtained are 22.0 ms and 36.5 respectively. For the frequency domain metrics, we obtained an error of 9.3 nu for the estimation of %LF (low frequency) and 0.4 for the LF/HF ratio. These results show that the proposed method outperforms other state of the art methods.**

***Index Terms*—Heart rate variability; Remote photoplethysmography; Telepsychiatry; Video Processing;**

I. Introduction

Depressive disorders are one of the leading causes of disability worldwide, affecting more than 4% of the world's population [1]. In addition, the recent COVID-19 pandemic caused a significant increase in mental health problems worldwide, which were exacerbated by the disruption of psychiatric assessments due to social distancing and quarantine measures. In this context, remote psychiatry consultations (i.e. telepsychiatry) can increase access to mental health services, reduce wait times, and reduce the burden on healthcare systems [2], [3].
Since the COVID-19 pandemic, teleconsultations have emerged as a reliable and effective method for remote diagnosis of depressive disorders. Moreover, the implementation of digital based tools with the goal of providing a non-invasive and accurate analysis of depression biomarkers could facilitate the diagnosis of depressive disorders. Examples of non-invasive and easily accessible biomarkers include measuring changes in heart rate (heart rate variability) and eye-blink rate.

A. Heart Rate Variability as a Biomarker for Depression

Heart Rate Variability (HRV) can be defined as the change in the time interval between two consecutive heartbeats. This variable is dependent on how the heart rate (HR) varies. This regulation/variation of HRV is done by the autonomic nervous system with the aim of ensuring optimal adaptation of HR to environmental challenges and unpredictable stimuli. [4].
Multiple studies reported that lower HRV, as well as the occurrence of abnormal HRV patterns are symptoms of depressive and mental disorders [5], [6]. Additionally, the continuous developments in the field of Remote Photoplethysmography (rPPG), which provides HR measures and analysis of HRV metrics through imaging, allows HR and HRV to be measured from a teleconsultation platform [7].
The relationship between HRV and depressive disorders is analyzed through time-domain and frequency-domain metrics that can be derived from the interval between two consecutive heartbeats (RR signal). Time-domain metrics of HRV quantify the amount of variability in the measurement of RR intervals with the most common measures being the standard deviation of RR Intervals (SDNN) and the root mean successive square difference (RMSSD). Frequency-domain metrics estimate the power spectral density of a given RR signal in different frequency bands. In the context of short-term recordings, the frequencies can be divided into three main bands [9]: very low frequency (VLF), which is comprised of rhythms with frequencies between 0.0033 and 0.04 Hz, low frequency (LF) which comprises of frequencies in a range e of 0.04-0.15 Hz and high frequency (HF) which comprises frequencies in a range of 0.15-0.40 Hz.
Several meta-analysis studies have analyzed HRV metrics in major depression, with results suggesting that patients suffering from depression are more likely to display reductions in HF, LF, VLF, RMSSD, SDNN and an increase in LF/HF ratio [10]–[12]. Altogether, these studies concluded that depressive disorders are associated with abnormalities in multiple HRV metrics.

B. Remote Photoplethysmography

Remote Photoplethysmography (rPPG) is a non-contact, remote method of measuring a person's heart rate using video recording. This measurement is based on subtle changes in facial skin color caused by the blood volume pulse (BVP).
In this report a rPPG chrominance based method is explored,

where a projection plane orthogonal to the skin tone is used for pulse extraction. This method is called the Plane-Orthogonal to Skin (POS) method andhas been validated to perform well in a teleconsultation context, where the individual remains stationary while speaking [13].
The basis of the POS method is a skin reflection model (**Fig. 1**) which, states that the color signal $\mathbf{C_k}(t)$ of the *k*th skin pixel at a given time *t* is dependent on the intensity of the light $I(t)$ that is reflected by the skin (Specular reflection $\mathbf{v_s}(t)$), as well as on the absorption and scattering of light in skin tissue (Diffuse reflection $\mathbf{v_d}(t)$), which depends on the amount of blood present in the blood vessels and the type of skin color of the individual. A quantization noise $\mathbf{v_n}(t)$ is also accounted for. The RGB color, $\mathbf{C_k}(t)$ signal can be defined through (1).

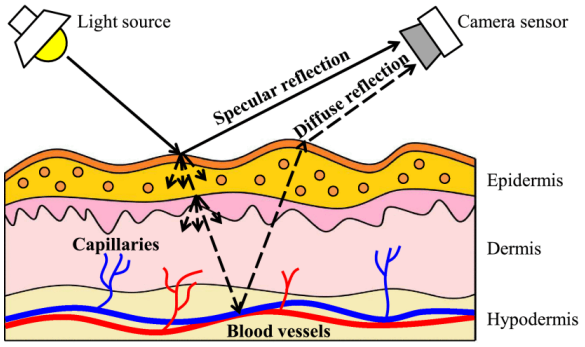

Fig. 1: Skin reflection model that contains both specular and diffuse reflections. Only the diffuse reflection contains pulsatile information. From [13].

$$\mathbf{C_k}(t) = I(t) \cdot \big(\mathbf{v_s}(t) + \mathbf{v_d}(t)\big) + \mathbf{v_n}(t) \tag{1}$$

The diffuse reflection term $\mathbf{v_d}(t)$, which varies with blood volume changes $p(t)$, and can be defined as:

$$\mathbf{v_d}(t) = \mathbf{u_d} \cdot d_0 + \mathbf{u_p} \cdot p(t) \tag{2}$$

where $\mathbf{u_d}$ denotes the unit color vector of the skin tissue, d_0 denotes the stationary reflection strength, $\mathbf{u_p}$ denotes the relative pulsatile strengths in RGB channels, and $p(t)$ denotes the pulse signal. From (1) and (2) we can define the problem of rPPG as extracting $p(t)$ from observations $\mathbf{C_k}(t)$.
In what follows, we propose an optimization of the digital signal processing pipeline presented by [7] to accomplish HRV measurements in the context of an augmented teleconsultation platform for depressive disorders. The key goal is to decrease computation time and memory required during signal processing. The precision and performance of the proposed method will be validated and compared with other state-of-the-art rPPG methods.

II. Methods

For optimization purposes, the proposed method works in real time, i.e. for each frame n being processed, the method only uses the current frame data as input. This means that there is no need to store previous frame data.
For a current frame n, we take as input a tuple of the form $(frame[n], timestamp[n])$, where $frame[n]$ is a $(width, height, 3)$ matrix storing the RGB intensities of each pixel of the current frame, and $timestamp[n]$ is the time at which the frame was captured. For each new frame, $(frame[n], timestamp[n])$ is updated with the values of the new frame.
Extracting HR and HRV measurements from a video requires five main steps: 1) region of interest (ROI) selection; 2) RGB signal extraction; 3) pulse signal extraction; 4) peak detection ; 5) HR and HRV calculations. An overview of the proposed method is shown in **Fig. 2**.

A. Region of interest selection and RGB signal extraction

The first step in HRV analysis is the selection of a region of interest (ROI) for each frame from which a pulse signal can be extracted. This ROI consists of the subject's cheeks, forehead and nose, as these are the regions where changes in the color signal caused by BVP are most pronounced. To select this ROI, we use the *dlib* machine learning library [14], where 68 facial landmark points are detected (**Fig. 3a**) using a method proposed by [15]. With these landmarks, it is possible to remove the unwanted regions and create a skin mask with our ROI (**Fig. 3b**).
Using the RGB intensities of each pixel in the ROI selected, the average intensities of each color component within the ROI are calculated for each frame n:

$$\mathbf{c}(n) = \begin{bmatrix} r(n) \\ g(n) \\ b(n) \end{bmatrix} \tag{3}$$

where $\mathbf{c}(n)$ denotes the average intensities of each color $r(n)$, $g(n)$ and $b(n)$ for the current frame n.

B. Pulse signal extraction

The POS methods is used for the pulse signal extraction [7]. This method, is a sliding window algorithm with a window length $l_f = f_S \cdot l_s$, where f_s is the sampling frequency, which is assumed to be constant over time, and l_s is the interval that contains one cardiac cycle, which is recommended to be 1.6 seconds.
In simple terms, the POS method consists of 3 main steps: 1) temporal normalisation; 2) orthogonal projection onto a plane orthogonal to the skin; 3) alpha-tuning to produce a one-dimensional pulse signal and 4) filtering of the pulse signal.

For each frame $n = 1, 2, ...N$,
$\mathbf{C}(n) = \big[\mathbf{c}(n - l_f), \ldots, \mathbf{c}(n)\big]$ is a 3xl_f matrix containing the average RGB values of the current sliding window. From this, we perform three steps:

1) Temporal Normalization: Temporal Normalization, the main goal is to eliminate the dependence of $\mathbf{C}(n)$ on the average skin reflection color

$$\widetilde{\mathbf{C}}(n) = diag^{-1}(\boldsymbol{\mu}(n)) \cdot \mathbf{C}(n) \tag{4}$$

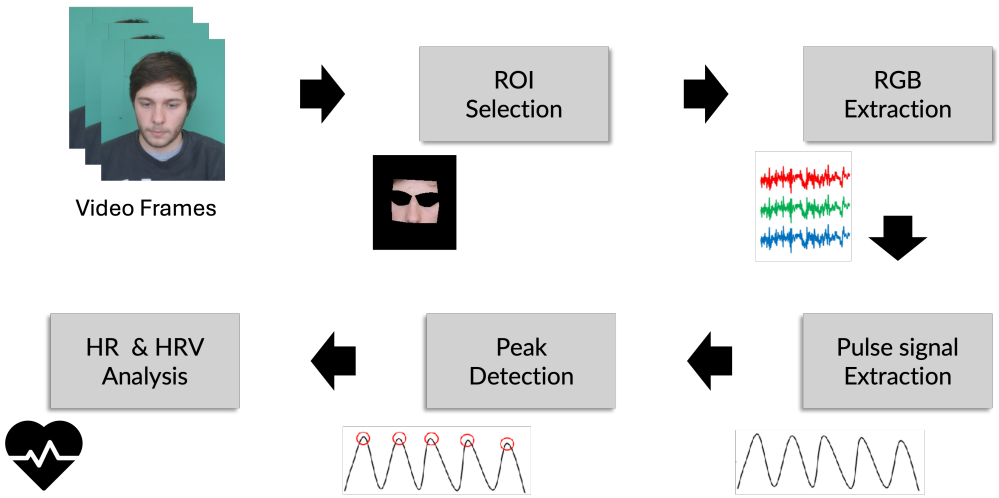

Fig. 2: Overview of the proposed method to extract HR and HRV measurements from a video recording of the face of a subject.

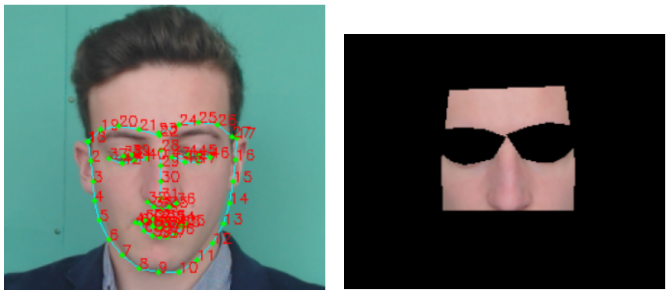

(a) (b)

Fig. 3: Dlib's 68-point facial landmark detection (a) and region of interest comprising cheeks, forehead and nose (b).

where $\boldsymbol{\mu}(n) = \left[\mu_{r(n)}, \mu_{g(n)}, \mu_{b(n)}\right]^\top$, denotes the temporal mean of the last l_f frames. $\widetilde{\mathbf{C}}(n)$ is a 3xl_f matrix with the normalized RGB values.

2) Orthogonal Projection: The next step consists in eliminating the intensity variations of $\widetilde{\mathbf{C}}(n)$ in the direction of $\left[1,1,1\right]^\top$ (**1**). To achieve this, [13] suggests projecting $\widetilde{\mathbf{C}}(n)$ onto the plane orthogonal to **1** by using a 2x3 projection matrix expressed as:

$$\mathbf{P} = \begin{bmatrix} 0 & 1 & -1 \\ -2 & 1 & 1 \end{bmatrix} \tag{5}$$

By multiplying $\mathbf{P}$ with the normalized RGB signal we generate a 2xl_f matrix $\mathbf{S}(n)$ containing two antiphase signals $\mathbf{s_1}$ and $\mathbf{s_2}$

$$\mathbf{S}(n) = \begin{bmatrix} S_1 \\ S_2 \end{bmatrix} = \mathbf{P} \cdot \widetilde{\mathbf{C}}(n) \tag{6}$$

3) Alpha-Tuning: Given the inphase/antiphase properties of $\mathbf{S}(n)$, alpha-tuning introduced by [16] is used to generate a pulse signal:

$$h(n) = S_1(n) + \alpha \cdot S_2(n) \text{ with } \alpha = \frac{\sigma(S_1)}{\sigma(S_2)} \tag{7}$$

where $\sigma(\cdot)$ is the standard deviation operator and $h(n)$ is a row vector containing the pulse signal values for the current sliding window.

4) Filtering: Finally, with the goal of performing HRV analysis, filtering the raw pulse signal is necessary for peak detection and HR calculation. Using the *SciPy* library [17], we implement a second order infinite impulse response (IIR) bandpass butterworth filter, with passband [0.8; 2.5] Hz which is the equivalent to a human heart rate range of 48 to 150 bpm (**Fig. 4**). The overall difference equation of the filtering process is the following:

$$\begin{aligned} y[n] = {} & 0.020 \cdot x[n] - 0.040 \cdot x[n-2] + 0.020 \cdot x[n-4] - 3.411 \cdot y[n-1] \\ & + 4.497 \cdot y[n-2] - 2.723 \cdot y[n-3] + 0.639 \cdot y[n-4] \end{aligned} \tag{8}$$

where $y[n]$ denotes the filtered signal obtained from $x[n]$ for the current frame n.

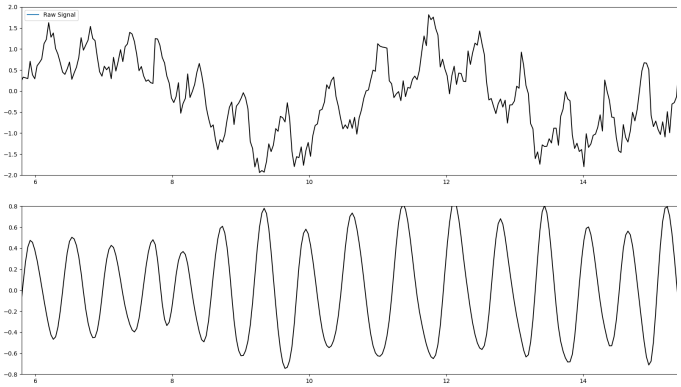

Fig. 4: Example of raw pulse signal extraction via POS method (upper method) and respective filtering (lower panel).

C. Algorithm Implementation

It is important to mention, that the POS method and [7] needs to store the last l_f RGB values in order to create a

pulse signal. This also means that a delay of 1.6 seconds is required to have enough data to start the algorithm.
With this in mind, we propose an algorithm optimization that only requires the current RGB values $\mathbf{c}(n)$.

Algorithm 1: Pulse signal extraction algorithm

Input: A video sequence containing N frames, l_f= 48 (30 fps video)

1: **for** $n = 1, 2, \ldots, N$ **do**

2: RGB pixel average: $\mathbf{c}(n) = \left[r(n), g(n), b(n)\right]^\top$

3: Temporal mean: $\boldsymbol{\mu}(n) \approx \frac{l_f-1}{l_f}\boldsymbol{\mu}(n-1) + \frac{1}{l_f}\mathbf{c}(n)$

4: Temporal Normalisation: $\widetilde{\mathbf{c}}(n) = diag^{-1}(\boldsymbol{\mu}(n)) \cdot \mathbf{c}(n)$

5: Projection: $\begin{bmatrix} s_1 \\ s_2 \end{bmatrix} = \mathbf{P} \cdot \widetilde{\mathbf{c}}(n)$

6: s_1 and s_2 mean: $\mu_{s_i} \approx \frac{l_f-1}{l_f}\mu_{s_{i-1}} + \frac{1}{l_f}s_i$

7: Variance calculation: $\sigma^2_{s_i} \approx \frac{\Delta_i^2}{l_f} + \frac{l_f-1}{l_f}\sigma^2_{s_{i-1}}$ with $\Delta_i = (s_i - \mu_{s_i})$

8: Alpha tuning: $h(n) = s_1 + \sqrt{\frac{\sigma^2_{s_1}}{\sigma^2_{s_2}}}s_2$

9: Normalisation: $H(n) = \frac{h(n)-\mu(h)}{\sigma(h)}$

10: **end for**

Output: The pulse signal H

D. Peak detection

The next step is to detect the systolic peaks of the filtered pulse signal. To do this, we use the *the mountaineer's method* [18], which has been proposed to deal with PPG signals regardless of their amplitude. This method is a point-by-point, *windowless* algorithm suitable for real-time applications. *The mountaineer's method* is programmed to detect true PPG peaks and ignore ripples. However, in some cases where the signal has abnormal peaks or is missing a peak, the method will detect these false peaks, resulting in incorrect HR calculations. As a solution, we propose a peak validation method that expects the next peak based on the previous HR estimates. From the last validated peak t_k, the next peak can be expected as:

$$t_{\text{expec}} = t_k + \mu_{T_k} \tag{9}$$

where μ_{T_k} denotes the mean of the current RR intervals. Initialized at 0.75 seconds (equivalent to a HR of 80 bpm), μ_{T_k} is updated every time a new peak is found:

$$\mu_{T_k} \approx \alpha T_k + (1-\alpha)\mu_{T_{k-1}} \tag{10}$$

here, $\alpha \in [0.6; 0.8]$, T_k denotes the last RR interval, and $\mu_{T_{k-1}}$ denotes the previous RR interval mean before t_k was validated. From this peak prediction, we search for possible peaks in the peak prediction window $[t_k + 0.5\mu_{T_k}, t_k + 1.5\mu_{T_k}]$.If only one peak is detected within the peak prediction window, that peak is marked as a validated peak. If no peaks fall within this window, we add a beat in t_{expec}. Otherwise, if multiple peaks $t_1, t_2, \ldots, t_y$ are detected within the peak prediction window, we calculate for each peak t:

$$P(t) = H(t)\frac{1}{\sqrt{2\pi}}e^{-\frac{(t-t_{\text{expec}})^2}{2}} \tag{11}$$

where $H(t_y)$ corresponds to the pulse signal value at the timestamp t_y. From (11), we choose the most appropriate peak, i.e., the largest peak that is closest to t_{expec}:

$$\text{Validated Peak} = \arg\max_{t \in \{t_1, t_2, \ldots, t_y\}} P(t) \tag{12}$$

In **Fig. 5**, we can observe an example of effective peak validation on an unstable pulse signal.

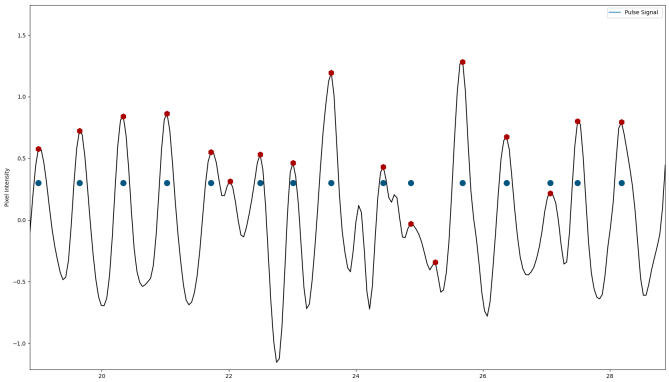

Fig. 5: Example of the proposed peak detection and validation on a unstable pulse signal. The red points correspond to the peaks detected by the mountaineer method. The blue points corresponds to the detected peaks validated by the proposed peak validation method. In this case, the mountaineer method detected unwanted peaks at around 22 and 25 seconds which were discarded by the validation method.

E. HR and HRV calculations

From the detected peaks we can build raw RR intervals from the difference between two consecutive peaks t_{k_i} and $t_{k_{i-1}}$.

$$RR_{interval_i} = t_{k_i} - t_{k_{i-1}} \tag{13}$$

With (13), a RR signal can be plotted (**Fig. 6**) over time where each point corresponds to the HR (in bpm) between two consecutive pulses
Finally, from the RR signal, we can obtain the HR and compute multiple HRV metrics over a specific time window w. The HR in bpm can be calculated as follows:

$$HR_w = \frac{60}{RR_w} \tag{14}$$

where RR_w is the mean of all RR intervals falling within the time window w. Using the *hrv-analysis* Python library [19] we compute two time-domain HRV metrics (SDNN and RMSSD) and three different frequency-domain metrics: normalised LF power, normalised HF power and LF/HF ratio. The results of the proposed method can be seen in **Fig. 7**

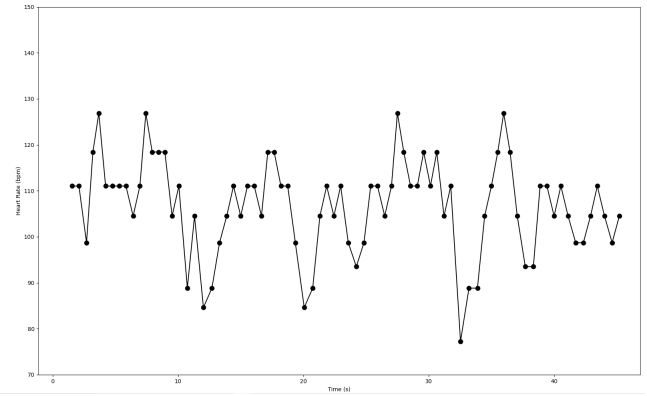

Fig. 6: Example of a RR signal in beats per minute over a time window of 40 seconds.

Fig. 7: The output of the pulse signal extraction algorithm. In the top left corner, we see multiple HR(PR long-term and PR instant) and HRV metrics (SDNN, RMSSD, LF, HF and LF/HF) for a 15 second window

F. Validation

To validate the proposed method, the *UBFC-RPPG video dataset* was used. This dataset consists of 40 videos, each with a corresponding PPG signal measured with a pulse oximeter finger clip sensor (ground truth). Each video is approximately one minute in length and was recorded using a 30 fps webcam. In these videos, the subjects sit in front of the camera in a teleconsultation-like context. For all 40 videos, all HRV and HR metrics were calculated for the entire recording, as well as HR for all 15 and 30 second time windows. These metrics were also calculated for the ground truth PPG signal. The performance of the proposed method was reported in terms of mean absolute error for all metrics:

$$MAE = \frac{\sum_{i=1}^{n} |x_i - y_i|}{n} \tag{15}$$

where x_i is the estimated metric and y_i is the ground truth.

III. Results and Discussion

A. Biomarker Validation

The algorithm used to optimize the digital signal processing pipeline presented by [7] was validated using the UBFC-RPPG video dataset. A summary of the performance of the method across all videos in the dataset is reported in I. When comparing HRV metrics to other state-of-the-art methods (Table II), the proposed method performs really well. In the case of the time-domain HRV metrics SDNN and RMSSD, the proposed method only performs worse to the one proposed by [21]. frequency-domain HRV metrics %LF and LF/HF, the proposed method outperforms FaceRPPG, the only method in the literature that reported those metrics

In the context of short-term human HRV features, these are reported to have the following ranges : SDNN ranges from 32-93 ms; RMSSD ranges from 19-75 ms; %LF (nu) ranges from 30-65 and LF/HF ranges from 1.1-11.6. From these ranges we conclude that %LF and LF/HF and SDNN are the most reliable features for medical application, since the average error of these metrics (10.48 (nu), 0.42 and 22.03) are smaller than their respective allowed ranges. On the other hand, the average error for RMSSD (35.57) is too large for this feature to be reliable since its range is almost as large as the allowed range.

Overall, the proposed method performed accurately in most videos (see example in **Fig. 8**). Due to good illumination and accurate skin mask selection, the extracted pulse signal only shows a slight delay relative to the ground truth signal. This delay is most likely due to certain delays in PPG signal acquisition or to the fact that the time it takes for blood to travel from the heart to the face is different from the time it takes for the blood to reach the fingers.

TABLE I: Average mean absolute error between ground truth and estimated heart rate and heart rate variability features across UBFC subjects. Rows are marked with asterisks according to the length of the analysis window used: * for 15-second window and ** for 30-second window.

	Average	**STD**
PR* (bpm)	1.70	2.78
PR (bpm)**	1.18	2.00
PR (bpm)	0.78	1.15
SDNN (ms)	22.03	26.70
RMSSD (ms)	35.57	27.06
LF (nu)	10.48	9.25
LF/HF	0.42	0.54

TABLE II: HRV estimation performance of in terms of mean absolute error for the UBFC dataset for different state-of-the-art methods: FaceRPPG [21], SSF [23] CHROM [22], [23], PulseGAN [22].

Method	FaceRPPG	SSF	CHROM	PulseGAN	Our method
SDNN (ms)	19	25	38.9	24.3	22.0
RMSSD	16	47	93		35.6
%LF	20				10.5
LF/HF	1.3				0.4

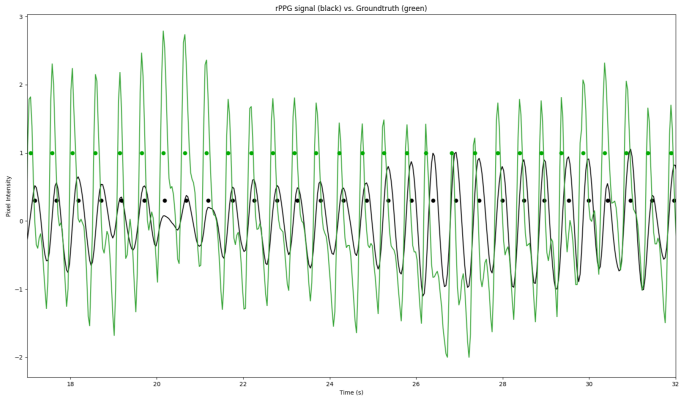

Fig. 8: Comparison between rPPG pulse signal and peaks (black) and the ground truth PPG signal of subject 34 of the UBFC-RPPG dataset.

In cases where, a high number of non-skin pixels (background, hair, glasses) are present in the skin mask, the extracted pulse signal is inaccurate. Consequently, the proposed method fails to make accurate HR and HRV estimations. Although the peak validation method is introduced to deal with pulse signal distortions, when the signal is degraded too much, the validation method performs poorly skipping or adding unwanted peaks (see example in **Fig. 9**). Additionally, if the subject's heart rate is naturally high ($>$115 bpm) at the beginning of the recording, the validation method can also perform poorly since the mean of the current RR intervals μ_{T_k}, is initialized assuming that the subject started with an HR of around 85 bpm.

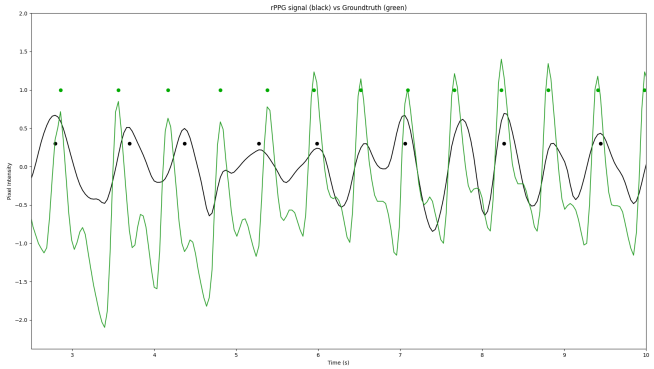

Fig. 9: Example of poor peak validation on a distorted pulse signal. The validation method is skipping peaks, because of a distorted peak at around 5 seconds.

B. Performance Analysis

To assess whether the proposed method performs better than the method used in [7], memory and time profiling was performed on a 68-second video from the UBFC-RPPG dataset. We obtained the total duration and memory used for both methods. As a control, we also performed memory and time profiling for the signal processing pipeline without performing HR and HRV estimations.

TABLE III: Example of time and memory profiling results obtained after pulse signal extraction from a 68-second video of the UBFC-RPPG dataset by different methods.

	Time (s)	Memory (MB)
No method	93.6	18.0
Old Method	102.9	22.9
Proposed Method	99.6	21.5

From Table III, we conclude that the proposed method is faster by 2.3 seconds and uses 1.4 MB less memory. These results were expected since the proposed method is simpler and only works with data from the current frame.

CONCLUSION

The analysis of heart rate variability metrics can aid doctors to remotely diagnose depressive disorders. Although several rPPG methods have been developed, it is important that these methods are simple and perform as efficiently as possible to improve their implementation in teleconsultation platforms. This report presents an optimization of a previous rPPG method that has already been implemented in a teleconsultation platform. The optimized method was validated using the UBFC-RPPG dataset, with results showing that it performs better when compared to other state-of-the-art methods.
As the proposed method has only been validated in an offline context, future work will aim to validate this method in a real-time context where the frame rate is not constant, in order to better simulate a teleconsultation environment.

REFERENCES

[1] M. J. Friedrich, "Depression is the leading cause of disability around the world," JAMA, vol. 317, no. 15, p. 1517, Apr. 2017.
[2] H. Li, A. Glecia, A. Kent-Wilkinson, D. Leidl, M. Kleib, and T. Risling, "Transition of mental health service delivery to telepsychiatry in response to COVID-19: A literature review," Psychiatr. Q., vol. 93, no. 1, pp. 181-197, Mar. 2022.
[3] A. Dawel, Y. Shou, M. Smithson, N. Cherbuin, M. Banfield, A. L. Calear, L. M. Farrer, D. Gray, A. Gulliver, T. Housen, S. M. McCallum, A. R. Morse, K. Murray, E. Newman, R. M. R. Harris, and P. J. Batterham, "The effect of COVID-19 on mental health and wellbeing in a representative sample of Australian adults," Frontiers Psychiatry, vol. 11, Oct. 2020.
[4] R. Acharya, U., K. Joseph, P., N. Kannathal, et al., "Heart rate variability: a review," Med. Biol. Eng. Comput., vol. 44, pp. 1031–1051, 2006.
[5] A. R. Brunoni, A. H. Kemp, E. M. Dantas, A. C. Goulart, M. A. Nunes, P. S. Boggio, J. G. Mill, P. A. Lotufo, F. Fregni, and I. M. Benseñor, "Heart rate variability is a trait marker of major depressive disorder: evidence from the sertraline vs. electric current therapy to treat depression clinical study," Int. J. Neuropsychopharmacol., vol. 16, no. 9, pp. 1937-1949, Oct. 2013.
[6] G. A. Alvares, D. S. Quintana, I. B. Hickie, and A. J. Guastella, "Autonomic nervous system dysfunction in psychiatric disorders and the impact of psychotropic medications: a systematic review and meta-analysis," J. Psychiatry Neurosci., vol. 41, no. 2, pp. 89-104, Mar. 2016.
[7] D. Ramalho, P. Constantino, H. P. D. Silva, M. Constante and J. Sanches, "An Augmented Teleconsultation Platform for Depressive Disorders," in IEEE Access, vol. 10, pp. 130563-130571, 2022.
[8] J. Sztajzel et al., "Heart rate variability: a noninvasive electrocardiographic method to measure the autonomic nervous system," Swiss medical weekly, vol. 134, no. 35-36, pp. 514–522, 2004.
[9] T. F. of the European Society Electrophysiology, "Heart rate variability," Circulation, vol. 93, no. 5, pp. 1043–1065, Mar. 1996. [Online].

[10] C. Koch, M. Wilhelm, S. Salzmann, W. Rief, and F. Euteneuer, "A meta-analysis of heart rate variability in major depression," Psychological medicine, vol. 49, no. 12, pp. 1948–1957, 2019.
[11] R. Hartmann, F. M. Schmidt, C. Sander, and U. Hegerl, "Heart rate variability as indicator of clinical state in depression," Frontiers in psychiatry, vol. 9, p. 735, 2019.
[12] J. Koenig, A. H. Kemp, T. P. Beauchaine, J. F. Thayer, and M. Kaess, "Depression and resting state heart rate variability in children and adolescents—a systematic review and meta-analysis," Clinical psychology review, vol. 46, pp. 136–150, 2016.
[13] W. Wang, A. C. den Brinker, S. Stuijk, and G. de Haan, "Algorithmic principles of remote PPG," IEEE Transactions on Biomedical Engineering, vol. 64, no. 7, pp. 1479–1491, Jul. 2017. [Online].
[14] D. E. King, "Dlib-ml: A machine learning toolkit," Journal of Machine Learning Research, vol. 10, pp. 1755–1758, 2009.
[15] V. Kazemi and J. Sullivan, "One millisecond face alignment with an ensemble of regression trees," in 2014 IEEE Conference on Computer Vision and Pattern Recognition. IEEE, Jun. 2014.
[16] G. de Haan and V. Jeanne, "Robust pulse rate from chrominance-based rPPG," IEEE Transactions on Biomedical Engineering, vol. 60, no. 10, pp. 2878–2886, Oct. 2013.
[17] E. Jones, T. Oliphant, P. Peterson et al., "SciPy: Open source scientific tools for Python," 2001–. [Online]. Available: http://www.scipy.org/
[18] E. J. Arg¨ uello-Prada, "The mountaineer's method for peak detection in photoplethysmographic signals," Revista Facultad de Ingenier´ıa Universidad de Antioquia, no. 90, pp. 42–50, 2019.
[19] R. Champseix, "Heart rate variability analysis," https://github.com/Aura-healthcare/hrv-analysis, 2020.
[20] S. Bobbia, R. Macwan, Y. Benezeth, A. Mansouri, and J. Dubois, "Unsupervised skin tissue segmentation for remote photoplethysmography," Pattern Recognition Letters, vol. 124, pp. 82–90, Jun. 2019.
[21] A. Gudi, M. Bittner, and J. v. van Gemert, "Real-time webcam heart-rate and variability estimation with clean ground truth for evaluation," Applied Sciences, vol. 10, no. 23, p. 8630, 2020.
[22] R. Song, H. Chen, J. Cheng, C. Li, Y. Liu, and X. Chen, "Pulsegan: Learning to generate realistic pulse waveforms in remote photoplethysmography," IEEE Journal of Biomedical and Health Informatics, vol. 25, no. 5, pp. 1373–1384, 2021.
[23] P. Li, Y. Benezeth, K. Nakamura, R. Gomez, C. Li, and F. Yang, "An improvement for video-based heart rate variability measurement," in 2019 IEEE 4th International Conference on Signal and Image Processing (ICSIP). IEEE, 2019, pp. 435–439.